10th International Electronic Conference on Synthetic Organic Chemistry (ECSOC-10). 1-30 November 2006. http://www.usc.es/congresos/ecsoc/10/ECSOC10.htm & http://www.mdpi.org/ecsoc-10/

[g001]

Polarizability Characterization of Zeolitic Brønsted Acidic Sites

Francisco Torrens[1] and Gloria Castellano[2,3]

[1]Institut Universitari de Ciència Molecular, Universitat de València, Edifici d'Instituts de Paterna, P. O. Box 22085, E-46071 València, Spain

[2]Departamento de Química, Universidad Politécnica de Valencia, Camino de Vera s/n, E-46022 València, Spain

[3]Departamento de Ciencias Experimentales, Facultad de Ciencias Experimentales, Universidad Católica de Valencia *San Vicente Mártir*, Guillem de Castro-94, E-46003 València, Spain

Abstract

The interacting induced-dipoles polarization model, implemented in our program POLAR, is used for the calculation of the effective polarizability of the zeolitic bridged OH group, which results much higher than that of the free silanol group. A high polarizability is also calculated for the bridged OH group with a Si^{4+}, in absence of Lewis-acid promotion of silanol by Al^{3+}. The crystal polarizability is estimated from the Clausius–Mossotti relationship. Siliceous zeolites are low-permittivity isolators. The interaction of a weak base with the zeolitic OH can be considered as a local bond. Only when cations are located in the zeolite micropore, next to tetrahedra that contain trivalent cations, are large electrostatic fields generated. They are short ranged, and the positive cation charges are compensated for by corresponding negative lattice charges. A method for the calculation of *fractal* surfaces of crystals is presented. The *fractal dimension D* of fragments of zeolites is calculated. Results compare well with reference calculations (GEPOL). The active site of Brønsted acid zeolites is modelled by sets of Al–OH–Si units, which form 2–12-membered rings. Topological indices for the different active-site models are calculated. The comparison between GEPOL and SURMO2 allows calculating the active-site indices. Most cavities show no fractal character, while for the 6–8-units rings *D* lies in the range 4.0–4.3. The 6-ring shows the maximum *D*; it is expected to be the most reactive.

Keywords: polarization; polarizability; active site; Brønsted acid; porous material; zeolite; fractal dimension; solvent-accessible surface.

Introduction

The catalytic properties of zeolites were determined by their framework composition [1]. Alteration of Si/Al ratio led to variations in the catalytic activity and stability of framework [2]. It was possible to substitute isomorphously certain elements into tetrahedral positions [3]. Isomorphously substituted zeolites showed variations in polarity and acidity, as well as became means by which to tailor them to suit catalytic needs. *Ab initio* calculations predicted structural and acidic properties of zeolites [4,5]. By using model-cluster units to represent a portion of the framework surrounding an active site, it was predicted the difference in acidity between a bridged Al hydroxyl (>OH) and a free or terminal –OH. They were included B [6], Ga and Ge isomorphously substituted forms, with the B and Ga forms corresponding to isomorphous substitution of Al, as well as the Ge form representing substitution of Si [7]. The calculated acidic characteristics were in good agreement with experiment. The use of zeolites as acidic catalysts raised interest in the structure and properties of their active sites [8,9]. The sources of Brønsted acidity in zeolites are bridged >OHs, which arise from Al or T^{III} atoms replacing Si [10]. The Brønsted acidity proton consists of an H atom, bonded to the O atom that connects the tetrahedrally coordinated cations (*cf.* Figure 1). Zeolites can be considered to be constructed of tetrahedra, with O atoms as apices and cations in the centre. The tetrahedra form a three-dimensional (3D) system by sharing of one O atom between each two tetrahedra. With Si^{4+} cations, the zeolitic framework is a polymorph of quartz and has SiO_2 stoichiometry. The zeolitic framework loses neutrality when lattice Si^{4+} become replaced by Al^{3+} cations. The excess lattice negative charge must be compensated for by positively charged cations. Usually alkali ions are used, which find a location in the microporous zeolite channel system. The zeolitic acidic site can be generated in several ways. NH_4^+ ions can be introduced in the zeolitic microcavity by ion exchange and, by heating, they can subsequently

be decomposed into NH_3 and H^+. The NH_3 molecule desorbs, and the proton is left bonded to a bridging lattice O atom, which connects a tetrahedron with a four-valent (Si^{4+}) cation and one that contains a three-valent (Al^{3+}, *etc.*) cation. Formally, the three-fold coordination of the O bridge is a nonclassical bonding situation also known, *e.g.*, H_3O^+. Compared to silanol (Figure 1a), which is only weakly acidic, the acidity of the proton is enhanced, which is due to a silanol that undergoes Lewis-acid promotion by Al^{3+}.

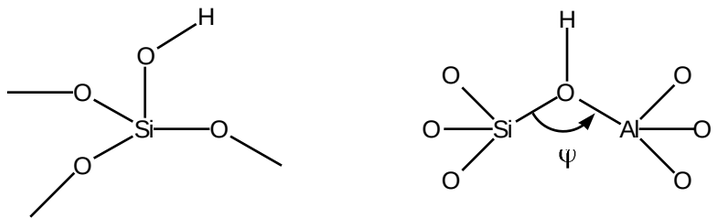

(a) (b)

Figure 1. Schematic representations of (a) silanol and (b) zeolitic Brønsted acidic hydroxyl.

Quantum-chemical calculations indicate that the charge of the proton is low (<0.1 e.u.) [11]. Proton nuclear magnetic resonance (NMR) data indicate a slight upward chemical shift compared to free silanol [12]. A small weakening of the O–H bond is demonstrated by a comparison of the stretching infrared (IR) frequencies. Whereas the silanol IR frequency is typically 3 750cm^{-1}, the zeolitic OH groups have frequencies between 3 550–3 650cm^{-1}. The stretching frequency of the zeolitic OH group is significantly higher than the highest lattice fundamental modes *ca.* 1 300cm^{-1}, which reflects the low proton mass. The group of Kazansky used the overtone spectrum of OH groups to deduce the potential of O–H using the Morse potential [13]. They found a covalent-dissociation energy of ~500kJ·mol^{-1}, with small differences in covalent-bond strength between OH groups on many different solids, which indicates that the acidic nature of the OH becomes apparent only when proton transfer itself, or the response of the OH on an interacting basic molecule, is measured. When the O–H bond is heterolytically broken (for an >OH the energy cost is ~1 250kJ·mol^{-1} [14]), the overall

bond energy will depend on the degree of stabilization of the negative charge left on the O atom. The silanol group (heterolytic-bond dissociation energy of 1 600kJ·mol^{-1}) is less acidic than the zeolitic OH, because the negative charge on the O atom is only stabilized by orbital interactions with one Si^{4+} ion in the case of the silanol, but by interactions with a Si^{4+} and another T^{3+} ion on the bridging site. The polarizability of the zeolitic OH is also much higher than that of the free silanol group. The polarizability relates to the electronic interactions between the O and neighbouring atoms. A classical interpretation of the high Brønsted acidity of the zeolite is the large Pauling-valency excess on the three-coordinated O atom. Whereas this valency excess is zero on the O atom of free silanol, it is +3/4 on the bridging zeolitic O atom, which represents the excess in effective formal positive charge of the nonclassically coordinated O atom. The simple electrostatic view of the zeolitic O–H bond can be misleading. The O–H and lattice O–T bonds must be considered as strong covalent bonds superposed by small (long-range) electrostatic interactions.

Apart from the analysis of the chemical bond of zeolitic materials, as obtained from electronic-structure calculations and direct computation of the electrostatic potential in the channels of the zeolite [15–17], the analysis of measured and computed vibrational spectra [18], as well as changes in bonding geometry upon protonation [19,20] provide additional information on the relative importance of electrostatic *vs*. covalent interactions. The difference in frequencies of the transversal and longitudinal optical modes in solids is a measure of the long-range electrostatic interaction in a solid. Whereas in high-symmetry crystals IR radiation only excites the transversal optical modes, the longitudinal modes are accessible by Raman or neutron excitation. The longitudinal modes, which correspond to atomic motions along a symmetry axis of a crystal, usually have a slightly higher frequency than transversal modes, which correspond to atomic motions perpendicular to a symmetry axis of a crystal. Long-range electrostatic interactions enforce themselves for longitudinal modes, but cancel each

other for transversal modes. The average difference of longitudinal and transversal optical-mode differences relates to the vibrational-plasmon frequency:

$$\langle \omega_{\mathrm{LO}} \rangle^2 - \langle \omega_{\mathrm{TO}} \rangle^2 = \langle \omega_{\mathrm{pl}} \rangle^2 \quad (1)$$

The vibrational plasmon is a collective charge oscillation. It is related to the elementary charge of the charge carriers and the permittivity of a solid:

$$\omega_{\mathrm{pl}}^2 = \frac{4\pi}{v\varepsilon(\infty)} \sum_i \frac{Q_i^2}{m_i} \quad (2)$$

where v is the molar volume, $\varepsilon(\infty)$, the permitttivity contribution due to electronic polarization, m_i, the atomic masses, and Q_i, the effective ionic charge. The computed vibrational-plasmon frequencies and measured values were compared for siliceous zeolitic polymorphs. The calculated values were obtained from extended-lattice calculations using rigid-ion, partial-charge or shell-model potential parameters. In the rigid-ion model, the charges on the ions are chosen to be equal to their formal valencies. The shell-model potential parameters are also based on formal valencies. Whereas polarization effects cannot be accounted for in the rigid-ion approximation, in the shell model the O atoms are considered polarizable. The shell model enables a prediction of $\varepsilon(\infty)$. Whereas the parameters used in the rigid-ion and shell models have been empirically obtained from the physical properties of quartz, the potential parameters of the partial-charge model have been estimated from the potential energy surfaces computed from *ab initio* calculations [21,22]. The charge on Si, according to partial-charge models, is approximately half of the formal valency. Both rigid-ion and shell models give too large long-range electrostatic interactions. Polarization effects reduce the contribution of the long-range electrostatic interactions, which have been also reduced in the partial-charge calculations due to the lower ionic charges, but are still too high because of the absence of polarization. The group of van Santen developed shell-potential parameters,

completely based on a fit to the potential energy surface and electrostatics from *ab initio* calculations on small clusters [23]. They had satisfactory agreement between computed and predicted permittivities. They calculated the large decrease in long-range electrostatic effects with a density decrease. For zeolites, *e.g.*, faujasite, long-range electrostatic interactions contribute only ~5% to the calculated vibrational-frequency differences [24]. In earlier publications, the fractal dimension of different structural-type zeolites was calculated; correlations were obtained between the fractal dimension and some topological indices [25]. Some Brønsted-acid models were proposed; the smallest unit SiH_3–OH–AlH_3 represented a bridged –OH, and the remaining models closed rings consisting of –SiH_2–OH–AlH_2– units [26]. Analyses of the geometric and topological indices for the active-site models were performed [27,28]. The aim of the present report is to perform a comparative study of the polarization properties of a set of Brønsted-acid models representative of Si–Al zeolites and to distinguish a particular ring that suggest greatest reactivity. In the next section the computational method is described. Following that the results are discussed. The last section summarizes the conclusions.

Results and Discussion

There exist more than one hundred zeolitic structures between natural and synthetic. These structures can be classified, *e.g.*, as a function of pore size or as a function of the orientation as well as the sort of channels and cavities that present. Three of the structures that are more used at industrial level are faujasite (FAU), mordenite (MOR) and ZSM-5 (MFI). Zeolites FAU are of large pore, forming almost spherical cavities of *ca.* 12Å of diameter interconnected by *windows* of 7.2Å. FAUs receive the name of type either X or Y according to the Al content of unit cell. FAUs with Al density between 77–96 Al/unit cell are of type X, and those with lower Al densities are type Y. Exchange cations are introduced to compensate the

charge defect generated by the substitutions of Al for Si atoms. Consequently, the number of exchange cations is greater in FAUs type X. Zeolites MOR are fundamentally formed by parallel channels, which present openings with small pores easy of blocking by materials outside the structure, *e.g.*, exchange cations. The lateral openings will influence the adsorption of small molecules, *e.g.*, methane, ethane or propane. Zeolites MFI present an intermediate pore size. MFIs consist of two perpendicular channel systems (straight and zigzag). MORs and MFIs contain between 0–8 Al/unit cell. Zeolites of six different structural types have been studied, *viz*. faujasite, ZSM-11, ZSM-5, mordenite, sodalite, and beta-A. The topological indices calculated for the zeolite crystals are reported (*cf.* Table 1), including two fragments of faujasite (I and II) with different numbers of atoms. The faujasite, ZSM-11, ZSM-5 and beta-A structures show 3D channels, while mordenite shows two-dimensional channels. Each type of zeolite possesses a well-defined crystalline structure with pores of distinct sizes. The studied zeolites cover different pore sizes: faujasite, mordenite and beta-A are large-pore zeolites (showing channels with access limited by 12-ring windows), while ZSM-11 and ZSM-5 (10-ring) as well as sodalite (6-ring) show smaller windows.

Table 1. Topological indices for zeolites.

Zeolite	D[a]	D'[b]	Framework density F_d[c]	Type of rings: R_{max}	Type of access	G[d]	G'[e]
Faujasite-I	1.866	2.317	12.7	12	3	0.326	0.838
Faujasite-II	1.912	2.193	12.7	12	3	0.295	0.864
ZSM-11	1.962	2.315	17.7	10	3	0.300	0.851
ZSM-5	2.026	2.174	17.9	10	3	0.295	0.867
Mordenite	1.961	2.058	17.2	12	2	0.317	0.882

Sodalite	2.149	2.311	17.2	6	3	0.225	0.934
Beta-A	1.981	2.215	15.1	12	3	0.276	0.825

[a] Fractal dimension of the solvent-accessible surface.

[b] Fractal dimension of the solvent-accessible surface averaged for non-buried atoms.

[c] The framework density is expressed as the number of T sites per 1000Å^3.

[d] Fragment globularity.

[e] Fragment rugosity (Å^{-1}).

The linear model graph for the fractal dimension D as a function of $\{F_d,R_{max},G,G'\}$ (*cf.* Figure 2) shows that the lineal model incorrectly predicts the fractal dimensions of ZSM-11 and ZSM-5. The quadratic model graph for D *vs*. $\{F_d,R_{max},G,G'\}$ is superposed on the original data (Figure 2).

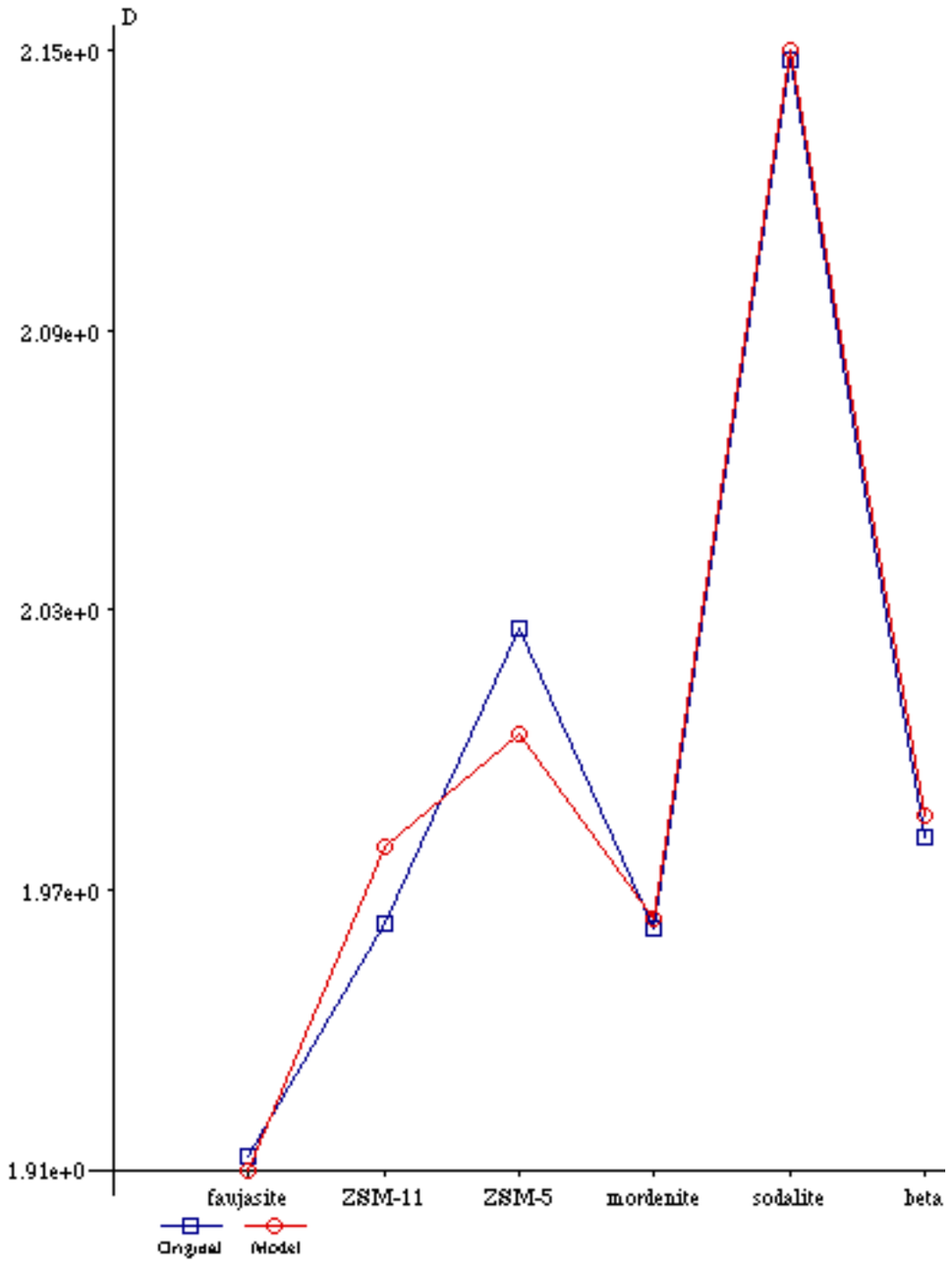

Figure 2. Comparison of the original data and the best linear model for the fractal dimension *D*.

The net group charge of silanol and zeolitic Brønsted acidic hydroxyls q_{OH} (*cf.* Table 2) has been calculated with AM1 and PM3. The inclusion of a bridged OH group in silanol [formal $Si(OH)_3–(O^+H)–Si(OH)_3$] causes an increase in both AM1 and PM3 q_{OH}. The corresponding interpretation is a bifurcated electronic transfer $Si(OH)_3 \leftarrow (OH) \rightarrow Si(OH)_3$, which is in agreement with the $>O^+H$ positive formal charge. Moreover, the subsequent

substitution of the second Si atom by Al [formal $Si(OH)_3–(O^+H)–Al^-(OH)_3$] produces an augmentation in AM1 q_{OH}, which represents a furhter electronic transfer $–(OH)\rightarrow Al(OH)_3$, in agreement with the $–(O^+H)–Al^-(OH)_3$ formal zwitterion. However, the result should be taken with care, because of a well-known limitation of AM1 for representing hydrogen bonding (H–bond), which is corrected in PM3. The >O–H…O(Si) contact is a van der Waals interaction, which can be considered a *weak* H–bond (d_{OO} = 2.345Å, $d_{O...H}$ = 2.273Å and angle OHO = 73.9º). The O–H…O interaction produces a decrease in PM3 q_{OH}, which represents a furhter electronic transfer >O–H←O(Si), favoured by a consequent transfer $O(Si)\rightarrow(OH)\rightarrow Al(OH)_3$.

Table 2. Net group charge (a.u.) of the bridged OH group.

Molecule	AM1[a]	PM3[b]
$Si(OH)_4$	-0.472	-0.321
$Si(OH)_3–(OH)–Si(OH)_3^+$	-0.443	-0.203
$Si(OH)_3–(OH)–Al(OH)_3$	-0.379	-0.220

[a] Calculations carried out with MOPAC–AM1.

[b] Calculations carried out with MOPAC–PM3.

The effective polarizability of silanol and zeolitic Brønsted acidic hydroxyls α_{OH} (*cf.* Table 3) has been calculated with our program POLAR. The inclusion of a bridged OH group in silanol causes a great increase in α_{OH}. Moreover, the subsequent substitution of the second Si atom by Al produces only a small augmentation in α_{OH}. The trend is in agreement with reference calculations carried out with our version of program PAPID.

Table 3. Effective polarizability (Å^3) of the bridged OH group.

Molecule	POLAR	Ref.[a]
$Si(OH)_4$	2.288	0.607
$Si(OH)_3$–(OH)–$Si(OH)_3^+$	5.162	0.926
$Si(OH)_3$–(OH)–$Al(OH)_3$	6.175	0.927

[a] Calculation carried out with program PAPID.

The high-frequency molecular polarizability $\alpha(\infty)$ calculated with the Clausius–Mossotti equation for siliceous zeolitic polymorphs (*cf.* Table 4) shows the moderate increase in long-range polarizability with a long-range permittivity increase, as well as the large decrease in long-range electrostatic effects and the moderate decrease in long-range polarizability with a density decrease of the system.

Table 4. High-frequency molecular polarizability $\alpha(\infty)$ calculated with Clausius–Mossotti equation.

Species	v (Å^3)	$\varepsilon(\infty)$	$\alpha(\infty)$ (Å^3)
α-Quartz *zz*[a,c]	37.66	2.383	2.837
α-Quartz *xx*[b,c]	37.66	2.356	2.799
Sodalite	56.17	1.699	2.535
Faujasite	74.07	1.503	2.539

[a] The *zz* component of the dielectric tensor and the shift of the A_2 modes are taken.

[b] The *xx* component of the dielectric tensor and the splitting of the E modes are taken.

[c] Experimental value.

A set of Brønsted-acid models representative of Si–Al zeolites is studied. The smallest unit investigated SiH_3–OH–AlH_3 is taken to represent a bridged hydroxyl group; the remaining active-site models are built by closing rings formed with 2–12 –SiH_2–OH–AlH_2– units. The internal cavities of these rings contribute to the total volume and fragment surface area. On the one hand, the total volume V_t of the active-site models of the zeolites is the sum of both fragment V_f and cavity V_c volumes: $V_t = V_f + V_c$. On the other, the fragment surface area S_f is the sum of both external S_e and cavity S_c surface areas: $S_f = S_e + S_c$. Table 5 lists the geometric descriptors for the active-site models. The calculations labelled fragment+cavity have been carried out with SURMO2. SURMO2 is unable to recognize the internal cavities of the active-site models. Hence the calculated volume V is a measure of the total volume V_t; *e.g.*, V_t(6-ring) = 567.3Å^3. Furthermore, GEPOL does recognize the cavities, and the value of the fragment volume V_f is available; *e*.g., V_f(6-ring) = 490.9Å^3. The external surface area S_e(6-ring) = 360.7Å^2 (SURMO2). Besides, the actual (external plus internal) fragment surface area S_f(6-ring) = 656.6Å^2 (GEPOL).

Table 5. Geometric descriptors for zeolite active-site models.

Type of ring	V[a] fragment +cavity	V[b] fragment	S[c] fragment +cavity	S[b] fragment	AS[d] fragment +cavity	AS[b] fragment	AS'[b,e] fragment
2	176.3	160.0	186.7	210.2	422.6	371.6	746.1
4	433.5	328.8	346.0	439.6	652.4	659.7	1106.0
6	567.3	490.9	360.7	656.6	854.9	992.2	1509.2
8	813.4	660.9	414.6	907.9	959.4	1363.3	2052.6
10	742.4	825.3	447.2	1135.5	910.9	1731.9	2631.2

12	888.2	989.2	460.7	1360.7	1062.9	2091.8	3203.6

[a] Fragment volume (Å^3).

[b] Calculations carried out with the GEPOL program.

[c] Fragment surface area (Å^2).

[d] Water-accessible surface area (Å^2).

[e] Side-chain accessible surface area (Å^2).

Table 6 reports the topological indices for the zeolite active-site models. The fragment globularity G is the topological index that better differentiates the active-site models. Not surprisingly, G is greater as calculated by SURMO2 (closer to unity for the largest ring in the $G_{\text{fragment+cavity}}$ column) compared with GEPOL (G_{fragment}). Moreover, the fragment rugosity G' is smaller. Notice that the internal cavity effect is difficult to appreciate in the context of the fragment volume, globularity and rugosity (10–12-ring), water-accessible surface (2-ring) and side-chain accessible surface area (2–6-ring), because of their small or null calculated cavity contributions.

Table 6. Topological indices for active-site models of zeolites.

Type of ring	G[a] fragment +cavity	G[b] fragment	G'[c] fragment +cavity	G'[b] fragment	D[d] fragment +cavity	D[b] fragment
2	0.814	0.678	1.059	1.313	1.262	1.324
4	0.800	0.524	0.798	1.337	1.372	1.501
6	0.919	0.458	0.636	1.337	1.372	1.598
8	1.016	0.404	0.510	1.374	1.261	1.603

10	0.887	0.375	0.602	1.376	1.305	1.595
12	0.970	0.353	0.519	1.376	1.268	1.587

[a] Fragment globularity.

[b] Calculations carried out with the GEPOL program.

[c] Fragment rugosity ($Å^{-1}$).

[d] Fractal dimension of the solvent-accessible surface.

From the calculation results referring to the total (SURMO2) and cavity-sensitive (GEPOL) fragment shape, they have been estimated the geometric descriptors and topological indices for the cavities of the active-site models of zeolites. The results (*cf.* Table 7) show that the cavity volume and surface areas are smaller for the 6-ring than for the 8-ring. However, for the 6-ring the globularity, rugosity and fractal dimension are greater. Notice that for the 2–8-ring cavities $S > AS \geq AS'$, because a water molecule with an effective radius of 1.41Å and a volume *ca.* $12Å^3$ can hardly be contained inside the smallest cavities. Moreover, a probe sphere representing a protein side chain, with a radius of 3.5Å and a volume *ca.* $180Å^3$, cannot be contained inside any of the cavities. For the 2–4- and 10–12-ring cavities, the fractal dimension D is *ca.* 2, indicating that the solvent-accessible surface of these rings is hardly sensitive to solvent size. Notwithstanding, for the 6–8-ring cavities, D lies in the range 4.0–4.3. In particular, the 6-ring cavity shows the greatest value of D, indicating the greatest sensitivity of the cavity accessible surface to solvent size. Therefore, it is suggested that the 6-ring cavity can have the greatest Brønsted-acid catalytic activity.

Table 7. Descriptors/indices for active-site model cavities.

Type of ring	V[a]	S[b]	AS[c]	AS'[d]	G[e]	G'[f]	D[g]

2	16.3	23.46	0.0	0.0	1.325	1.439	2.000
4	104.7	93.56	7.3	0.0	1.148	0.894	2.000
6	76.4	295.92	137.3	0.0	0.294	3.873	4.271
8	152.5	493.34	403.9	45.3	0.280	3.235	3.951
10	0.0	688.28	821.0	819.7	0.000	∞	1.985
12	0.0	899.99	1028.9	1103.3	0.000	∞	1.943

[a] Cavity volume ($Å^3$).

[b] Cavity surface area ($Å^2$).

[c] Water-accessible surface area ($Å^2$).

[d] Side-chain accessible surface area ($Å^2$).

[e] Cavity globularity.

[f] Cavity rugosity ($Å^{-1}$).

[g] Fractal dimension of the solvent-accessible surface.

Figure 3 shows the variation of the side-chain accessible surface area (AS') with the water-accessible surface area (AS) of the zeolite active-site models for the 1–12-ring. Three points (1-, 2- and 4-ring) appear superposed.

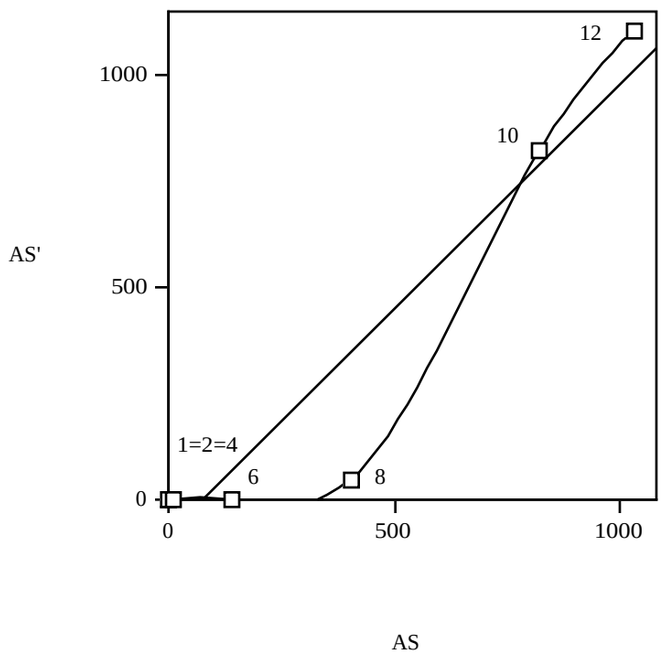

Figure 3. Side-chain- *vs*. water-accessible surface areas of active-site models of zeolites.

The linear fit corresponds to:

$$AS' = -80.0 + 1.05AS \qquad r = 0.953 \qquad (9)$$

The slope indicates that an increase of 1.00Å^2 in AS corresponds to an increase of 1.05Å^2 in AS'. The abscissa (or the intersection with the interpolation line) at AS = 76.2Å^2 is closer to the 6-ring, indicating the greatest sensitivity of its solvent-accessible surface to solvent size.

The atom-to-atom analysis of the geometric descriptors and topological indices for the zeolite 6-ring active-site model, carried out with TOPO, considers (*cf.* Table 8) four atoms, *viz*. Si, O, H(O), and Al, in each –SiH_2–OH–AlH_2– unit. The greatest contribution to the ring volume V comes from each Si atom (52% of that for Si/O/H/Al). The same trend has been observed for the surface area S_{Si} (50%), as well as solvent-accessible surface areas AS_{Si} (76%) and AS'_{Si} (53%), due to the greatest accessibility of each Si atom (Acc_{Si} = 20.3%). The Si-atom term in the ring globularity G_{Si} is the lowest. Moreover, each Si-atom component part in

the ring rugosity G'_{Si} is small. Each Si-atom input to the ring fractal dimension D_{Si} is low; however, for the O atoms D_O is the greatest and for the Al atoms D_{Al} is large. The ring cavity contributes to the total volume and surface area, as explained above (Table 6). Again, $S_{cavity} > AS_{cavity} \geq AS'_{cavity}$ as expected for a small cavity. The fractal dimension D_{cavity} is large, indicating the sensibility of the solvent-accessible surface of the cavity to solvent size and suggesting that this cavity can have large Brønsted-acid catalytic activity. The ring rugosity G' and accessibility are small. The ring fractal dimension D is large.

Table 8. Geometric and topological indices for zeolite 6-ring active-site model: Atomic analysis.

Atom	V[a]	S[b]	G[c]	G'[d]	AS[e]	Accessibility[f]	AS'[g]	D[h]
Si	26.1	26.59	1.602	1.017	29.0	20.3	10.3	3.022
O	6.5	6.49	2.591	1.001	3.2	3.6	0.1	5.749
H(O)	7.7	9.09	2.076	1.179	3.2	3.5	8.9	2.963
Al	9.8	11.41	1.941	1.164	2.9	3.2	0.1	5.594
Cavity	76.4	295.92	0.294	3.873	137.3	–	0.0	4.271
All ring	487.9	624.64	0.480	1.280	965.7	18.4	1490.6	1.584

[a] Ring volume ($Å^3$).

[b] Ring surface area ($Å^2$).

[c] Ring globularity.

[d] Ring rugosity ($Å^{-1}$).

[e] Water-accessible surface area ($Å^2$).

[f] Accessibility (%) of the water-accessible surface.

[g] Side-chain accessible surface area ($Å^2$).

[h] Fractal dimension of the solvent-accessible surface area.

Our results, indicating the maximal sensibility of the solvent-accessible surface of the 6-ring cavity to solvent size, are in agreement with Hammonds *et al.* rigid-unit crystal vibrational mode (RUM) model for the binding site of cations [39]. In faujasite, the 6-ring was calculated to be opening and closing under the influence of a local RUM, in agreement with experiments.

From the present results the following conclusions can be drawn.

1. The polarizability of the zeolitic OH group is much higher than that of the free silanol group. Moreover, a high polarizability is also calculated for the bridged OH group with a Si^{4+} cation, even in absence of Lewis-acid promotion of silanol by Al^{3+}.

2. Siliceous zeolites are isolators with a low permittivity. The interaction of a weak base with the zeolitic OH can be considered as a local bond, which is similar to the hydrogen bonding that occurs between gas-phase acidic molecules, *e.g.*, $HCl–NH_3$. Only when cations, *e.g.*, Na^+, K^+ or Mg^{2+} and Ca^{2+}, are located in the zeolite micropore next to tetrahedra that contain trivalent cations, *e.g.*, Al^{3+} instead of Si^{4+}, are large electrostatic fields generated. They are short ranged, and the positive cation charges are compensated for by corresponding negative lattice charges.

3. The utilization of the arranged porous solids requires high area and cavities interconnected on various size scales. Therefore, the use of synthesis methods, which allow tailoring porosity without the necessity for great experimental complexity, must permit the preparation of the amounts of homogeneous material necessary for large-scale applications. However, as important is the cavity as the atoms that form it, so that the advances in the selective functionalization of the surface must allow the design of materials with specific functions. As it could be varied the surface composition and could be manipulated the microstructure of the zeolitic skeleton, new properties will be found.

4. The fragment globularity G is the topological descriptor that better differentiates the zeolite active-site models. The 6-membered-ring cavity model of the zeolite active site shows the greatest fractal dimension, indicating the greatest sensitivity of its solvent-accessible surface to solvent molecular size. Therefore, it is suggested that the 6-ring can have the greatest activity as acidic catalyst. Work is in progress to check the validity of this result.

General procedure

The α dipole–dipole polarizability is calculated with the interacting induced-dipole polarization model [29], which calculates effective anisotropic point polarizability tensors by the method of Applequist *et al.* [30]. The $\alpha_{ab}^{\mathrm{mol}}$ molecular polarizability is defined as the linear response to an external electric field,

$$\mu_a^{\mathrm{ind}} = \alpha_{ab}^{\mathrm{mol}} E_b^{\mathrm{ext}} \tag{3}$$

where μ_a^{ind} is the induced molecular dipole moment and a, b, c… denote Cartesian components [31–33]. Considering a set of N interacting atomic polarizabilities, the atomic induced-dipole moment has a contribution also from the other atoms,

$$\mu_{p,a}^{\mathrm{ind}} = \alpha_{p,ab}\left(E_b^{\mathrm{ext}} + \sum_{q\neq p}^{N} T_{pq,bc}^{(2)}\mu_{q,c}^{\mathrm{ind}}\right) \tag{4}$$

where $T_{pq,bc}^{(2)}$ is the interaction tensor

$$T_{pq,ab}^{(2)} = \frac{3r_{pq,a}r_{pq,b}}{r_{pq}^5} - \frac{\delta_{ab}}{r_{pq}^3} \tag{5}$$

where r_{pq} is the distance between atoms p and q, and δ represents the Kronecker δ function: $\delta(a,b) = 1$ if $a = b$, and $\delta(a,b) = 0$ if $a \neq b$. The molecular polarizability can then be written as

$$\alpha_{ab}^{\mathrm{mol}} = \sum_{p}^{N}\alpha_{p,ab}^{\mathrm{eff}} = \sum_{q,p}^{N} B_{pq,ab} \tag{6}$$

where α^{eff}_p is the effective polarizability of atom *p*, and **B** is the relay matrix defined as (in a supermatrix notation)

$$\mathbf{B} = \left(\alpha^{-1} - T^{(2)}\right)^{-1} \tag{7}$$

The difference between our program POLAR and our version of PAPID [34,35] is in the different parametrization scheme used for the initial atomic polarizabilities. PAPID uses atomic α_p values fitted to high-quality calculations, while POLAR performs a simpler individual computation for each molecule, in order to exploit the difference among different atoms in different functional groups in different molecular environments.

An optimized version of our program POLAR, including the whole interacting induced-dipole polarization model, has been implemented in the program molecular mechanics (MM2), its extension to transition metals (MMX) and empirical conformational energy program for peptides (ECEPP2). The new versions are called MMID2 [36], MMXID [37] and ECEPPID2 [38].

The crystal polarizability is estimated by the Clausius–Mossotti relationship:

$$\alpha = \frac{3(\varepsilon - 1)v}{4\pi(\varepsilon + 2)} \tag{8}$$

where v is the elementary volume per molecule in the crystalline state, and ε is the relative permittivity. The high-frequency molecular polarizability $\alpha(\infty)$ represents the molecular polarizability contribution due to electronic polarizability $e(\infty)$.

Acknowledgement. We wish to thank Dr. C. M. Zicovich-Wilson for providing us with calculation results before publication on the optimized geometry of zeolites. The authors acknowledge financial support from the Spanish MEC DGI (Project No. CTQ2004-07768-C02-01/BQU), Generalitat Valenciana (DGEUI INF01-051 and INFRA03-047, and OCYT GRUPOS03-173) and Universitat de València–Mediscovery.

References

[1] J. A. Rabo, Ed., Zeolite Chemistry and Catalysis, American Chemical Society, Washington, 1976.

[2] G. T. Kerr, Adv. Chem. Ser., 219 (1973).

[3] R. M. Barrer, Hydrothermal Chemistry of Zeolites, Academic, New York, 1982, p. 287.

[4] W. Mortier, J. Sauer, J. A. Lercher and H. Noller, J. Phys. Chem. **88**, 905 (1984).

[5] J. G. Fripiat, F. Berger-André, J. M. André and E. G. Derouane, Zeolites **3**, 306 (1983).

[6] P. J. O'Mailley and J. Dwyer, J. Chem. Soc., Chem. Commun. 72 (1987).

[7] P. J. O'Malley and J. Dwyer, Chem. Phys. Lett. **143**, 97 (1988).

[8] H. W. Haynes, Jr., Catal. Rev.–Sci. Eng. **17**, 273 (1978).

[9] P. A. Jacobs, Catal. Rev.–Sci. Eng. **24**, 415 (1982).

[10] P. Viruela-Martín, C. M. Zicovich-Wilson and A. Corma, J. Phys. Chem. **97**, 13713 (1993).

[11] J. Sauer, Chem. Rev. **89**, 199 (1989).

[12] H. Pfeifer, D. Freude and M. Hunger, Zeolites **5**, 274 (1985).

[13] V. B. Kazansky, Acc. Chem. Res. **24**, 379 (1991).

[14] H. V. Brand, L. A. Curtiss and L. E. Iton, J. Phys. Chem. **97**, 12773 (1993).

[15] C. Pisani, J. Mol. Catal. **82**, 229 (1993).

[16] V. R. Saunders, C. Freyeria-Fava, R. Dovesi, L. Salasco and C. Roetti, Mol. Phys. **77**, 629 (1992).

[17] E. Aprà, R. Dovesi, C. Freyeria-Fava, C. Pisani, C. Roetti and V. R. Saunders, Mod. Sim. Mater. Sci. Eng. **1**, 297 (1993).

[18] W. P. J. H. Jacobs, J. H. M. C. van Wolput, R. A. van Santen and H. Jobic, Zeolites **14**, 117 (1994).

[19] Z. Jirak, V. Vratislav and V. Bosacek, Phys. Chem. Solids **41**, 1089 (1980).

[20] M. Czjzek, H. Jobic, A. Fitch and T. Vogt, J. Phys. Chem. **96**, 1535 (1992).

[21] B. W. H. van Beest, G. J. Kramer and R. A. van Santen, Phys. Rev. Lett. **64**, 1955 (1990).

[22] S. Tsuneyuki, M. Tsukada, H. Aoki and Y. Matsui, Phys. Rev. Lett. **61**, 869 (1988).

[23] K. de Boer, A. P. J. Jansen and R. A. van Santen, Chem. Phys. Lett. **223**, 46 (1994).

[24] A. J. M. de Man, B. W. H. van Beest, M. Leslie and R. A. van Santen, J. Phys. Chem. **94**, 2524 (1990).

[25] F. Torrens, Top. Catal. **18**, 291 (2002).

[26] F. Torrens, Comput. Mater. Sci. **27**, 96 (2003).

[27] F. Torrens, Mol. Phys. **100**, 3105 (2002).

[28] F. Torrens and G. Castellano, J. Nanomater., in press.

[29] L. Silberstein, Philos. Mag. **33**, 92 (1917).

[30] J. Applequist, J. R. Carl and K.-K. Fung, J. Am. Chem. Soc. **94**, 2952 (1972).

[31] F. Torrens, J. Sánchez-Marín and I. Nebot-Gil, J. Mol. Struct. (Theochem) **463**, 27 (1999).

[32] F. Torrens, J. Phys. Org. Chem. **15**, 742 (2002).

[33] F. Torrens, J. Comput. Methods Sci. Eng. **4**, 439 (2004).

[34] C. Voisin, A. Cartier and J.-L. Rivail, J. Phys. Chem. **96**, 7966 (1992).

[35] C. Voisin and A. Cartier, J. Mol. Struct. (Theochem) 286, 35 (1993).

[36] F. Torrens, M. Ruiz-López, C. Cativiela, J. I. García and J. A. Mayoral, Tetrahedron **48**, 5209 (1992).

[37] F. Torrens, Polyhedron **22**, 1091 (2003).

[38] F. Torrens, Mol. Simul. **24**, 391 (2000).

[39] K. D. Hammonds, V. Heine and M. T. Dove, J. Phys. Chem. B **102**, 1759 (1998).